



Virginia Commonwealth University
VCU Scholars Compass

Chemistry Publications

Dept. of Chemistry

2007

Control of the cation occupancies of MnZn ferrite synthesized via reverse micelles

M. D. Shultz

Virginia Commonwealth University

M. J. Allsbrook

Virginia Commonwealth University

E. E. Carpenter

Virginia Commonwealth University, ecarpenter2@vcu.edu

Follow this and additional works at: http://scholarscompass.vcu.edu/chem_pubs

 Part of the [Chemistry Commons](#)

Shultz, M. D., Allsbrook, M. J., & Carpenter, E. E. Control of the cation occupancies of MnZn ferrite synthesized via reverse micelles. *Journal of Applied Physics*, 101, 09M518 (2007). Copyright © 2007 American Institute of Physics.

Downloaded from

http://scholarscompass.vcu.edu/chem_pubs/19

This Article is brought to you for free and open access by the Dept. of Chemistry at VCU Scholars Compass. It has been accepted for inclusion in Chemistry Publications by an authorized administrator of VCU Scholars Compass. For more information, please contact libcompass@vcu.edu.

Control of the cation occupancies of MnZn ferrite synthesized via reverse micelles

M. D. Shultz, M. J. Allsbrook, and E. E. Carpenter^{a)}

Department of Chemistry, Virginia Commonwealth University, 1001 W. Main Street, Richmond, Virginia 23284

(Presented on 9 January 2007; received 2 November 2006; accepted 28 December 2006; published online 8 May 2007)

Variations in cation occupancy in mixed metal ferrite systems can affect their electronic and magnetic properties. It is known that different synthesis parameters can lead to various cation distributions and the ability to tune these distributions is of great interest. This study uses the extended x-ray-absorption fine structure-IR relationship to investigate the effect of various $\text{Fe}^{2+}/\text{Fe}^{3+}$ ratios in initial synthesis conditions on cation distribution for manganese zinc ferrite (MZFO). Differences in the precipitated material before firing could lead to differences in the final material if fired under similar conditions. This work uses several different ratios of $\text{Fe}^{3+}/\text{Fe}^{2+}$, which will affect the initial cell potential for the reaction, to synthesize nano MZFO. All samples were fired for 5 h at 500 °C under flowing nitrogen. Transmission electron microscopy micrographs reveal highly crystalline uniform nanoparticles of 16 ± 2 nm. The x-ray diffraction revealed single phase crystalline MZFO with an average crystallite size of around 14 nm. The saturation magnetization ranged from 43 to 68 emu/g as measured by vibrating-sample magnetometry. The Fourier transform infrared (FTIR) analysis was used to determine the cation occupancies while changing the initial $\text{Fe}^{3+}/\text{Fe}^{2+}$ ratios from 10/90 to 90/10. The FTIR spectra revealed a shift in the first absorption region in the far IR from 566.98 to 549.62 cm^{-1} corresponding to the octahedral occupancies. This shift corresponds to a change in the percentage of octahedral sites occupied by manganese from roughly 25% to 12%. This change in manganese occupancy is also observed in the iron occupancies, which in turn help to explain the variation in saturation magnetization. © 2007 American Institute of Physics. [DOI: 10.1063/1.2713694]

The purpose of this study was to investigate the hypothesis that cation distribution in manganese zinc ferrites (MZFOs) is a tunable property. The ability to specifically and consistently tailor MZFO that possess desired electronic and magnetic properties is of great interest. The cation distribution throughout the octahedral and tetrahedral sites in the spinel structure greatly influences these properties;^{1,2} thus it is important to determine an adjustable synthesis parameter that can be used to control the cation occupancies, creating the optimal MZFO for the desired applications. Here we examine the differences in cation occupancy and zinc incorporation in MZFO nanoparticles and present a synthesis parameter that allows for variation of these characteristics.

MZFO nanoparticles were synthesized via reverse micelle techniques utilizing nonylphenoxy poly(ethyleneoxy)ethanols with differing head group repeating units of 7 and 4 as surfactant and cosurfactant (NP7/NP4).^{3,4} The metal hydroxides were precipitated at room temperature while employing Schlenk line techniques under N_2 . One reverse micelle microemulsion containing aqueous FeCl_2 , FeCl_3 , MnCl_2 , and ZnCl_2 was quickly added to a second microemulsion containing 4 mL of concentrated NH_4OH in order to rapidly raise the pH and precipitate the metal hydroxides. In typical ferrite format, the mole ratios of the metals used were as follows: $\text{MnCl}_2=0.5$, $\text{ZnCl}_2=0.5$, and $\text{FeCl}_x=2$, (X

$=2,3$). The only variable that was varied between samples was the initial Fe^{3+} and Fe^{2+} molar ratio with the sum always equal to 2, relative to the other metals. Samples were then washed in air with methanol, collected by centrifugation, and dried in a vacuum oven at room temperature. The dry material was then annealed in a tube furnace under flowing nitrogen for 5 h. Powder x-ray diffraction showed pure crystalline MZFO phase, with a slight phase impurity in the 90/10 sample. Figure 1 shows the diffraction pattern for 80/20, which is comparable to all other samples, and the diffraction pattern for 90/10. The small peak and shouldering pointed to

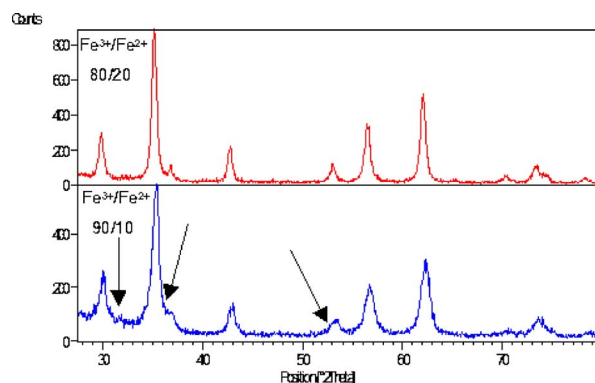


FIG. 1. Powder x-ray diffraction pattern of 80/20 sample (top), which is similar to all other samples, and the diffraction pattern for 90/10 (bottom). The arrows point to shouldering and a small peak at $2\theta \approx 32$, which are indicative of a ZnO impurity.

^{a)}Author to whom correspondence should be addressed; electronic mail: ecarpenter2@vcu.edu

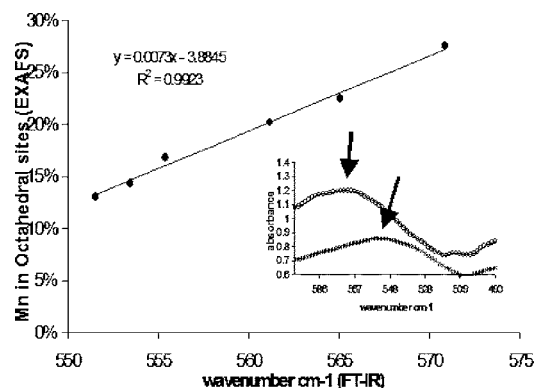


FIG. 2. Plot of the percentage of the available octahedral sites occupied by Mn vs wave number. This same peak in the far IR is also correlated with the octahedral Fe occupancy and yields the same occupancy results shown in Table I.

in Fig. 1 are indicative of some form of zinc oxide (ZnO). This impurity will have a greater effect on the magnetic characterization due to the magnetic dilution with an antiferromagnetic impurity than on the actual cation occupancy analysis since the Zn impurity retains tetrahedral coordination. Scherrer analysis revealed an average crystallite size of 14 nm and transmission electron microscopy (TEM) images confirmed a nanomorphology consistent with this size.

Magnetic characterization was performed on a vibrating-sample magnetometer at room temperature. Elemental analysis was carried out on a Varian Vista-MPX ICP-OES, with the samples dissolved in nitric acid by use of a 23 mL Parr Instrument Company microwave acid digestion bomb. Fourier transform infrared (FTIR) spectra were collected on a Nicolet Nexus 670 FTIR with a polyethylene beam splitter, deuterated triglycine sulfate (DTGS) detector, and a purge cell apparatus to minimize moisture in the measuring environment. Sample preparation and spectra analysis were performed in the same manner as previously described.⁵

In order to elucidate how the initial $\text{Fe}^{3+}/\text{Fe}^{2+}$ ratio affects the cation distribution in nanoscale MZFO, we em-

ployed a FTIR method that allows for fast determination of the cation occupancies due to a correlation between vibrational modes in the far-IR region, and extended x-ray-absorption fine structure (EXAFS) determined octahedral manganese occupancy.⁵ Figure 2 shows this correlation, which has been adjusted from the previous work by the addition of a data point that had been used as a validation sample. The wave number values in Table I correspond to the maximum in the center of the first absorption region in the far-IR spectra from 600 to 200 cm^{-1} for each sample (sample IR data in the inset of Fig. 2). Inserting these values into the equation seen in Fig. 2 yields the fraction of octahedral sites occupied by $\text{Mn}^{2+/3+}$. Assuming that all of the Zn^{2+} resides in tetrahedral sites,² these values can then be used along with the stoichiometric ratios determined by elemental analysis to obtain the full cation distribution (Table I).

Magnetic characterization was then performed to corroborate the calculated cation distributions. It is known that the magnetic moments of the tetrahedral (A) sites and the octahedral (B) sites display an antiparallel orientation for Fe_3O_4 .² For this inverse spinel structure, there are twice as many B sites than A sites, thus there is a resultant magnetic moment. Since the Mn incorporation is constant, the Zn and the Fe exchange positions. With the substitution of “nonmagnetic” ions such as Zn into the lattice, this leads to an increase in saturation magnetization. Experimentation has shown that, in the case of MZFO, the maximum in saturation magnetization is reached at the stoichiometry of $\text{Mn}_{0.5}\text{Zn}_{0.5}\text{Fe}_2\text{O}_4$.² Since all of the samples seen in Table I have less total $\text{Mn}^{2+/3+}$ and Zn^{2+} incorporation than 1.0, the saturation magnetization should be more reliant on the fraction of tetrahedral sites occupied by Fe^{3+} . Indeed this is the trend seen in Fig. 3, where the saturation magnetization is decreased with increasing tetrahedral Fe^{3+} .

In the FTIR calculations, it was observed that as the initial $\text{Fe}^{3+}/\text{Fe}^{2+}$ ratio increased from 10/90 to 90/10, the fraction of octahedral sites occupied by $\text{Mn}^{2+/3+}$ decreased from 0.25 to 0.12 while maintaining a consistent level of

TABLE I. Results from FTIR analysis, relative stoichiometry of metals by ICP-OES listed in conventional ferrite formula (AB_2O_4), calculated cation distribution in the fraction of A and B sites occupied, and observed XRD purity.

| Initial $\text{Fe}^{3+}/\text{Fe}^{2+}$ ratio | 10/90 | 30/70 | 50/50 | 60/40 | 70/30 | 80/20 | 90/10 |
|--|--------|--------|--------|--------|--------|--------|--------|
| Wave number (cm^{-1}) | 566.98 | 563.12 | 555.41 | 553.48 | 551.55 | 549.62 | 549.62 |
| Stoichiometry (ICP) | | | | | | | |
| Mn | 0.49 | 0.47 | 0.49 | 0.48 | 0.50 | 0.54 | 0.42 |
| Zn | 0.36 | 0.24 | 0.19 | 0.20 | 0.30 | 0.25 | 0.42 |
| Fe | 2.16 | 2.29 | 2.32 | 2.33 | 2.20 | 2.21 | 2.16 |
| Calculated occupancy: | | | | | | | |
| Tetrahedral (A) Mn | 0.00 | 0.01 | 0.15 | 0.16 | 0.22 | 0.30 | 0.18 |
| Tetrahedral (A) Zn | 0.36 | 0.24 | 0.19 | 0.20 | 0.30 | 0.25 | 0.42 |
| Tetrahedral (A) Fe | 0.65 | 0.75 | 0.66 | 0.65 | 0.48 | 0.45 | 0.40 |
| Octahedral (B) Mn | 0.25 | 0.23 | 0.17 | 0.16 | 0.14 | 0.12 | 0.12 |
| Octahedral (B) Fe | 0.75 | 0.77 | 0.83 | 0.84 | 0.86 | 0.88 | 0.88 |
| XRD purity | Good | Good | Good | Good | good | Good | Fair |

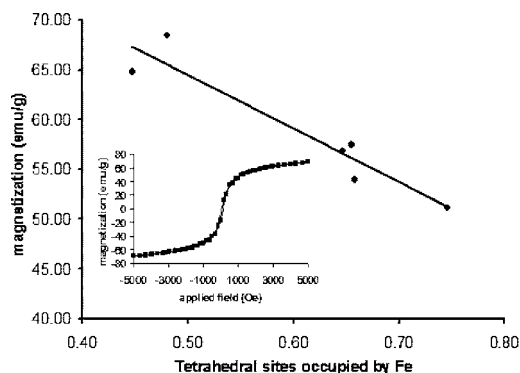


FIG. 3. Saturation magnetization is plotted vs the fraction of tetrahedral sites occupied by Fe. The inset is an example of the hysteresis plot obtained by VSM. (Note that data from the initial ratio of 90/10 was excluded due to the phase impurity seen in the x-ray diffraction pattern.)

incorporation in the ferrite. In contrast, the Zn^{2+} showed a changing level of incorporation into the ferrite with a minimum value at 50/50 (Fe^{3+}/Fe^{2+}). A plot of the fraction of tetrahedral site occupied by Zn^{2+} can be seen in Fig. 4.

The explanation for these two trends can be found when contemplating the differences in the hydroxides precipitated during the synthesis. Starting initially with more Fe^{2+} than Fe^{3+} , the precipitation goes through a green to black color change. Under oxygen deficient conditions, the green color indicates the formation of green rust, which in the presence of Cl^- will form chlorine-containing green rust,^{6,7} in which the Fe is in two different types of coordination sites. One of these sites is identical to pure $Fe(OH)_2$ with a coordination to six OH^- , and the other with a coordination to five OH^- and one Cl^- .⁷ The solubility of $ZnCl_2$ typically involves the Zn^{2+} bridged between Cl^- anions.⁸ This would then allow for the Zn^{2+} to be more easily incorporated into this expanded lattice of the precipitated green rust due to Cl^- inclusion in the structure. Next during the methanol washing in air, the green rust is converted to an iron oxyhydroxide via oxidation, in which the Cl is removed and replaced by O, thus disrupting the lattice and allowing for the Zn to migrate into tetrahedral sites. Finally, upon annealing under flowing N_2 , the presence of two Fe sites and more Zn^{2+} then drives most of the into octahedral sites. This is noted by the calculated absence of tetrahedral $Mn^{2+/3+}$ shown in Table I. Also during the firing, with the Zn^{2+} is already in the lattice, the $Fe^{2+/3+}$ migrates to octahedral sites leaving the Zn^{2+} to fulfill the charge balance.

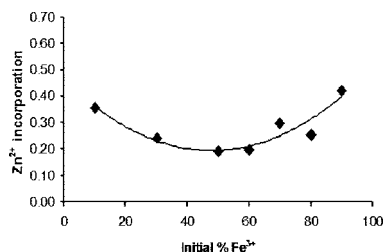


FIG. 4. Plot of stoichiometric fraction of Zn^{2+} vs the initial percentage of Fe^{3+} , which, due to the assumption that all of the Zn^{2+} is tetrahedral because of a strong electronic preference for these sites, can also be viewed as the fraction of tetrahedral sites occupied by Zn^{2+} .

At the opposite end of the spectrum, when starting with a greater abundance of Fe^{3+} , the reaction proceeds through an orange to black color transition. The orange color is indicative of a predominantly $Fe(OH)_2$ form of iron hydroxide, which is a tetrahedral deficient structure with the Fe^{3+} being coordinated to six OH^- . Since Fe^{3+} has a greater affinity for OH^- than Fe^{2+} , and has a greater affinity for OH^- than for Cl^- , the Cl^- is not incorporated into this structure. Also, with lack of divalent cations in the system for charge balance in the spinel and the fact that Zn can also coordinate to four OH^- in this type of complex $[Zn(OH)_4]^{2+}$,⁸ the Zn^{2+} is more easily incorporated into the ferrite upon annealing. The number of octahedral sites occupied by $Mn^{2+/3+}$ is also lowest at the higher Fe^{3+}/Fe^{2+} ratios due to more Fe^{3+} initially occupying octahedral sites and the need for more divalent cations to fill the tetrahedral sites. One important feature to keep in mind is that all of the samples were fired for 5 h under flowing N_2 . It is known that there is an interconversion type equilibrium between $Mn^{2+/3+}$ and $Fe^{3+/2+}$,⁹ and thus with extended firing times, it may be possible for more $Mn^{2+/3+}$ to be incorporated into the octahedral sites. Since the temperature of annealing used in this study is fairly low for ferrites and the time of annealing was held constant and is somewhat short, we were able to discover this trend.

To explain the minimum Zn^{2+} incorporation at the Fe^{3+}/Fe^{2+} ratio of 50/50, a combination of the two hydroxide forms must exist during the precipitation reaction. This suggests that there would be less tetrahedral and divalent cation deficiencies than in the high Fe^{3+} case, and less Cl^- incorporation in the structure to possibly allow for more Zn^{2+} inclusion than in the high Fe^{2+} case. During the washing steps, there would already be a substantial amount of divalent and trivalent cations present, along with the reduced presence of Cl, resulting in less disruption during the firing process causing slower migration of the Zn^{2+} into the lattice. This then supports the result that less Zn^{2+} was found in the 50/50 sample and the parabolic type relationship between initial Fe^{3+}/Fe^{2+} and Zn^{2+} incorporation.

With the results found in this study, it would be possible to better formulate the mechanism behind cation migration and incorporation during the MZFO synthesis. Such a mechanistic understanding would allow for specific tailoring of a desired cation distribution in MZFO, leading to more efficient industrial synthesis and the optimal MZFO.

The authors would gratefully like to thank the Thomas Jeffress and Kate Jeffress Memorial Trust and PM-USA INEST group for funding.

¹S. A. Morrison *et al.*, J. Nanosci. Nanotechnol. **5**, 1323 (2005).

²J. Smit and H. P. J. Wijn, *Ferrites: Physical Properties of Ferrimagnetic Oxides in Relation to Their Technical Applications* (Wiley, New York, 1959).

³S. Calvin *et al.*, Phys. Rev. B **66**, 224405 (2002).

⁴S. A. Morrison *et al.*, J. Appl. Phys. **93**, 7489 (2003).

⁵M. D. Shultz *et al.*, J. Appl. Phys. **99** (2006).

⁶I. R. McGill *et al.*, Nature (London) **259**, 200 (1976).

⁷P. H. Refait *et al.*, Corros. Sci. **40**, 1547 (1998).

⁸F. A. Cotton and G. Wilkinson, *Advanced Inorganic Chemistry*, 5th ed. (Wiley, New York, 1988).

⁹D. J. Fatemi *et al.*, J. Appl. Phys. **83**, 6867 (1998).